Photoacoustics 28 (2022) 100421

Contents lists available at ScienceDirect

Photoacoustics

journal homepage: www.elsevier.com/locate/pacs

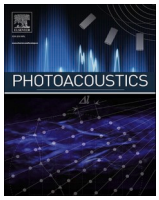

Miniaturized fiber optic ultrasound sensor with multiplexing for photoacoustic imaging

Liuyang Yang [a,b], Dongchen Xu [a], Geng Chen [a], Anqi Wang [a], Liangye Li [a], Qizhen Sun [a,b,*]

[a] School of Optical and Electronic Information & National Engineering Research Center of Next Generation Internet Access-system (NGIAs) & Wuhan National Laboratory for Optoelectronics (WNLO), Huazhong University of Science and Technology, Wuhan, Hubei 430074, China
[b] Hust-Wuxi Research Institute, Wuxi, Jiangsu 214174, China

ARTICLE INFO

Keywords:
Optical fiber
Parallel detection
Coherent demodulation
Ultrasound sensor
Photoacoustic imaging

ABSTRACT

A miniaturized ultrasound sensor based on optical fiber is designed and realized for multichannel parallel ultrasound detection and photoacoustic imaging. The fiber optic sensor is composed of a polymer coating, a reflective mirror and a single-mode optical fiber, with only 125 μm in diameter. By integrating the coherent demodulation technology and multiplexing technology, which using a relatively cheap fixed wavelength laser, hundreds of sensors could work simultaneously. Meanwhile, highly sensitive ultrasound detection has been demonstrated with the noise equivalent pressure as low as 0.46 kPa and the sensor exhibits a nearly omnidirectional directivity. Furthermore, a photoacoustic imaging system based on three sensors working in parallel is demonstrated. High lateral resolutions of 165–217 μm and axial resolutions of 112–131 μm over a depth range of larger than 5 mm are obtained. A three-dimensional phantom imaging experiment is also demonstrated. Benefited from parallel detection, the imaging speed is three times faster than that of a single sensor. The miniaturized fiber optic ultrasound sensor probe provides a competitive alternative for mechanically scanning-free endoscopic imaging, which is beneficial from small size, omnidirectional directivity and parallel detection capability.

1. Introduction

Photoacoustic imaging technology is an emerging method which is based on optical absorption with ultrasound resolutions [1,2]. Compared with other existing imaging techniques, photoacoustic imaging provides high resolution, deep penetration depth and excellent optical contrast, simultaneously [3,4]. In photoacoustic imaging systems, short laser pulses are illuminated onto biological tissue to excite photoacoustic waves. Chromophores such as hemoglobin [5], melanin [6] or contrast media [7] in tissue will be heated by absorbing photons and then generate ultrasound signals through thermoelastic expansion. After distributed detection of the ultrasound signals, the image of light absorption distribution can be reconstructed [8,9]. In order to accurately capture the ultrasound signals, ultrasound sensors with excellent performance are needed, where the piezoelectric sensors represent the current state of the art. However, piezoelectric sensors have several limitations as follows. Firstly, the piezoelectric sensor is sensitive to ambient electromagnetic disturbances due to electrical loading effects. This can result in the piezoelectric sensor fails to work in the harsh environment with strong electromagnetic interference. And the detection limit scales of piezoelectric sensor approximately inversely with the piezoelectric element size. Especially for high resolution imaging based on high acoustical frequency, this imposes an insufficient detection sensitivity, which can deteriorate the signal-to-noise ratio and fidelity of image. In addition, piezoelectric sensors are usually fabricated from acoustically resonant piezoceramic materials, which suffer from limited bandwidth around resonance frequency. This precludes a faithful representation of the incident ultrasound wave and ultimately reduces the resolution of image.

Ultrasound detection via fiber optic sensors is a promising field, and a number of different optical fiber sensing schemes have been developed in recent years [10–15]. Among them, fiber optic resonant structures for ultrasound sensors have strong competivity [12,16–18], due to the outstanding performances of high sensitivity and smaller size. In theory, the sensor structures including polymer-membrane based Fabry-Perot interferometers (FPI) [12,19], fiber gratings[15,20] and micro-ring

* Corresponding author at: School of Optical and Electronic Information & National Engineering Research Center of Next Generation Internet Access-system (NGIAs) & Wuhan National Laboratory for Optoelectronics (WNLO), Huazhong University of Science and Technology, Wuhan, Hubei 430074, China.
E-mail address: qzsun@mails.hust.edu.cn (Q. Sun).

https://doi.org/10.1016/j.pacs.2022.100421
Received 22 December 2021; Received in revised form 29 September 2022; Accepted 24 October 2022
Available online 25 October 2022

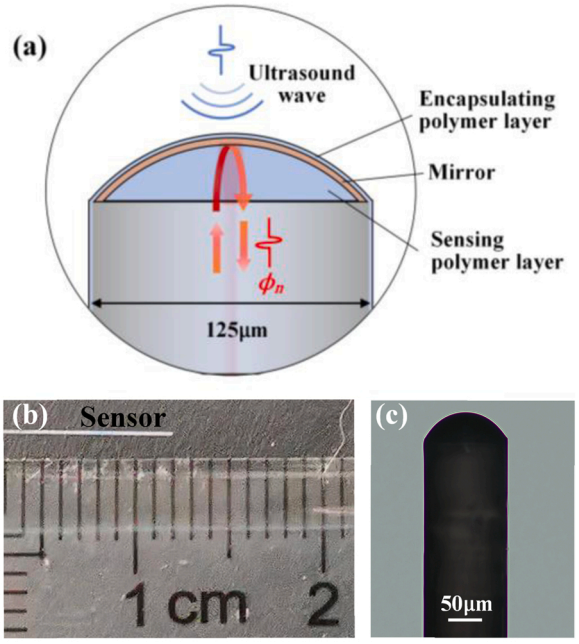

Fig. 1. (a) Schematic diagram of the fiber optic ultrasound sensor. Photograph (b) and micrograph (c) of the fiber optic ultrasound sensor probe.

resonators[17] have extremely high sensitivity with a very small footprint owing to the long interaction length. The spectral sideband filter technique is commonly used to achieve signal demodulation for ultrasound detection [21–23]. While the technology relies on expensive tunable laser to track the highest slope of cavity transfer function, which makes the system costly. Meanwhile, mechanical scanning of ultrasound probe is required for imaging, which limit the imaging speed. Several imaging systems without mechanical scanning have been reported, which employ large scale fiber bundle with FPI deposited on the fiber end face [24,25]. However, the system still interrogates FPIs one by one, due that fabricating multiple FPIs with identical cavity lengths face great challenge [26]. The optimum operating wavelength of different FPIs are inconsistent, which eliminates the possibility of large scale multiplexing to improve the imaging speed.

Interferometric fiber sensor is another type that is widely used for ultrasound detecting[11,13,27]. Compared with resonant sensors, interferometric sensors have lower demodulation cost and better multiplexing capability. The Mach-Zehnder interferometer and Michelson interferometer with simple structures are the most common ultrasound detection schemes[28,29]. The interrogation of these ultrasound sensors employs a single-wavelength laser, which provides a feasible solution for parallel ultrasound detection of multiple fiber sensors. For example, a 64 channel photoacoustic imaging system with coherent demodulation technique has been built and used for high frame rate photoacoustic imaging [11]. However, the interferometric sensor is not compact, resulting in the narrow directivity and poor spatial resolution. Besides, its sensitivity mainly depends on the length and material of sensing fiber, which leads to an undesirable sensitivity. Thus, compact and highly sensitive ultrasound sensors are of great desirable for wide applications in photoacoustic imaging and beyond.

In this work, we propose a miniaturized fiber optic ultrasound probe with the diameter of only 125 μm, through coating a high elastic polymer layer and a reflective mirror on the end face of single mode fiber. With the help of coherent demodulation technique, the signal from sensor can be captured with high sensitivity using a low-cost single-wavelength laser. Multichannel parallel ultrasound detection capability and nearly omnidirectional directivity are experimentally demonstrated. Besides, a prototype of photoacoustic imaging system is developed and successfully applied for 2D and 3D high resolution photoacoustic imaging.

2. Sensor fabrication and operation principle

The schematic diagram of the fiber optic ultrasound sensor is shown in Fig. 1(a). To fabricate the sensor, a single mode fiber is cut by a fiber cleaver. Then the cleaved fiber is fixed in a customized dip-coater and the end-face of the fiber is parallel to the UV glue surface. Lower the fiber so that the fiber end-face is immersed into the UV glue to a depth about 2 mm. Afterwards, with a moving velocity of 50 μm/s, the fiber is pulled out the UV glue. A certain amount of UV glue is collected on the end face of fiber and forms a curved polymer coating. The amount of UV glue build-up at the fiber tip is determined by the viscosity of the UV glue and the speed of pulling. Therefore, the thickness of polymer coating can be controlled by adjusting these parameters. The UV glue attached on the fiber tip is cured by an UV lamp for 2 h and aged for 1 week. After aging, a 100 nm thick gold reflective film is deposited on the sample surface using vacuum evaporation process. Finally, the sample is coated with another layer polymer film using dip-coating method to prevent water immersion. It should be noticed, the reflectivity of the interface between the optical fiber and the polymer is much lower than that of the gold mirror, so the interference caused by the reflected light can be ignored. Since the sensor is built on the end-face of optical fiber, the size of sensor depends on the optical fiber. Fig. 1(b) and (c) shows

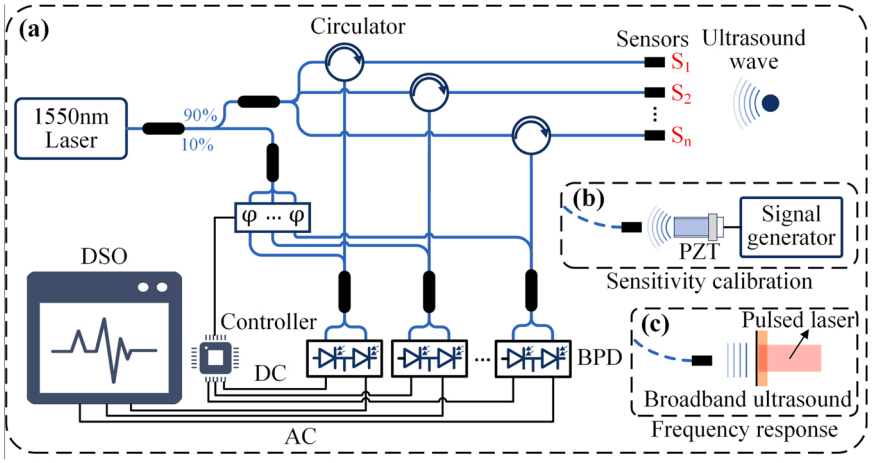

Fig. 2. (a) Schematic of the ultrasound detection system; (b) Sensitivity calibration; (c) Frequency response. DSO: Digital oscilloscope; φ: Phase modulator; BPD: Balance photodetector; AC: Alternating current; DC: Direct current; PZT: Piezoelectric transducer.

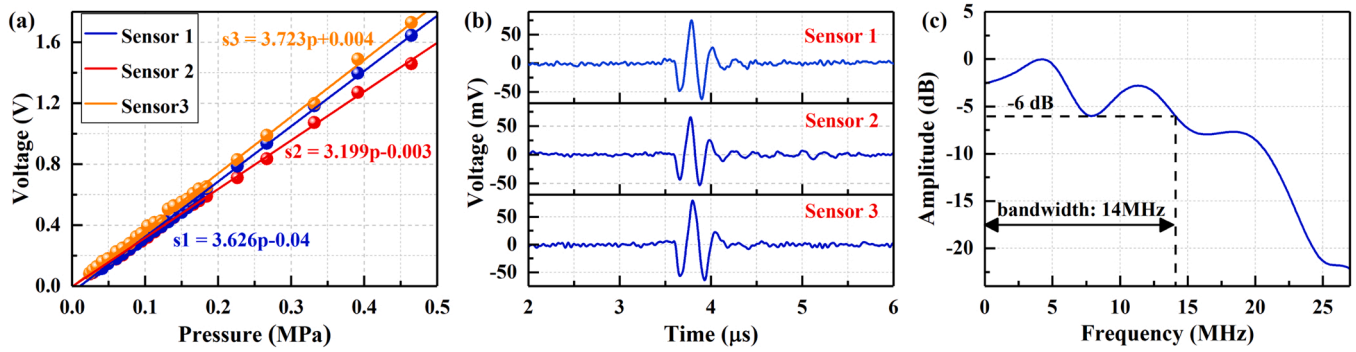

Fig. 3. (a) Ultrasound pressure sensitivity of the fiber sensors. (b) Output signals from three sensors. (c) Frequency response of the sensor.

the photograph and micrograph of the fiber optic sensor with a diameter of 125 μm.

When ultrasound wave is applied on the sensor tip, the thickness of polymer coating changes accordingly, resulting in the optical path change of interrogation light. In this way, the optical phase modulation of the reflected interrogation light from the polymer coating is achieved. According to ref [21], the relationship between phase shift of nth sensor's interrogation light $d\phi_n$ and incident acoustic pressure P_n can be expressed as

$$d\phi_n = \frac{4n}{\lambda}\frac{\lambda_a}{E}\sin\left(\frac{2\pi l_n}{\lambda_a}\right)P_n \tag{1}$$

Where λ_a and λ represent the wavelength of acoustic wave and interrogation light, respectively. n and E denote the refractive index and Young's modulus of the polymer material, respectively. l_n is the polymer coating thickness of the nth sensor. Then, the coherent intensity demodulation method is used to convert the phase shift into the light intensity changes, which exhibits linear relationship by setting the initial static operating point at the quadrature point. The acoustic sensitivity S_n can be derived as the following equation

$$S_n = 4\sqrt{I_1 I_2}\,\frac{d\phi_n}{P_n} = 4\sqrt{I_{n1} I_{n2}}\,\frac{4n}{\lambda}\frac{\lambda_a}{E}\sin\left(\frac{2\pi l_n}{\lambda_a}\right) \tag{2}$$

Where I_{n1} and I_{n2} are the optical intensities of the probe and the reference light of the nth sensor in Section 3.1, respectively. Therefore, the proposed sensor with smaller Young's modulus and higher refractive index will have a higher ultrasound sensitivity.

3. Ultrasound measurement

3.1. System setup

The system configuration of the ultrasound measurement is illustrated schematically in Fig. 2. Due that the phase changes caused by the incident ultrasound wave is extremely weak, coherent intensity detection technique for improving the signal-to-noise ratio is employed for the fiber optic ultrasound sensor. Hence, a Mach-Zehnder interferometer (MZI) with phase feedback mechanism is used for signal demodulation. The fixed wavelength laser with narrow linewidth outputs continuous light of 1550.12 nm, which is split into the probe light and the reference light by an 90%:10% coupler to improve interference contrast. To interrogate the sensors simultaneously, the probe light and reference light are divided into multiple channels, respectively. Limited by the experimental devices available in the laboratory, three channels are demonstrated in this work. Each probe light launches into a fiber optic ultrasound sensor through a circulator. The reflected light from the sensor is carried with incident acoustic signal and interfered with a reference channel. The interference signal is received and converted to electric signal by a balanced photodetector (BPD), and then the electric signal is split to alternating current (AC) and direct current (DC) signal. The AC signal represents the incident ultrasound signal and the DC signal indicates the slow shift of the MZI working-point. To achieve optimal sensitivity, the system has to operate at the quadrature point, where the phase difference between probe light and reference light is $\pi/2$. Phase modulators and a homemade controller are employed to stabilize the operating point of the reference channel. By adopting the Proportion Integration Differentiation (PID) controlling scheme, the phase of reference light can be dynamically adjusted by feeding the DC signal to the controller. In this way, the system always operates in the quadrature point and the phase vibration caused by the incident ultrasound wave can be linearly translated to the light intensity change. Briefly, the pressure of incident ultrasound signal is proportional to the amplitude of AC signal, which is digitized and recorded through an oscilloscope.

3.2. Characterization of the ultrasound sensor

To demonstrate the multichannel parallel ultrasound detection ability of the system, three sensors with polymer coating thickness of 24.7 μm, 22.4 μm and 25.8 μm are fabricated. The sensitivity of fiber optic ultrasound sensors is calibrated using a 5 MHz unfocused ultrasound transducer. The generated pressure of the transducer is calibrated using a commercial (Polyvinylidene fluoride) needle hydrophone (NH200, Precision Acoustics). In this calibration, the distance between the ultrasound transducer and the fiber optic ultrasound sensor is about 5 mm, which is the same as the distance between ultrasound transducer and commercial needle hydrophone. The voltages of output signals with different pressures and exhibited in Fig. 3(a). Linear fitting is used to calculate the sensitivity of the sensors. The result shows good linearity and similar sensitivity, which provides feasibility for parallel ultrasound detection of multi-sensors [30]. The slight inconsistency of sensitivity is caused by the differences in polymer coating thickness and the reflectivity of mirrors.

The typical measured signals of three sensors is shown in Fig. 3(b) when the pressure is 40 kPa. The output signals from three sensors exhibit similar waveforms. To evaluate the noise equivalent pressure (NEP), the acquired data with 1 μs before the ultrasound signal arrived is used to assess the noise level, the root-mean-square noise level is 1.6 mV over a 20 MHz measurement bandwidth. The output signal of sensor 1 shows a peak-to-peak value of 138 mV, and the corresponding NEP is 0.46 kPa, which is about three times lower than that of the commercial hydrophone. Although the NEP of the proposed sensor is approximately a factor of 11 higher than the FPI ultrasound sensor[31], the large-scale multiplexing capability still offers potential applications in rapid photoacoustic imaging. In addition, the NEP of the sensor can be further reduced by using polymer with lower Young's modulus and interrogation laser with lower relative intensity noise and narrower linewidth.

In order to measure the frequency response of the fiber optic ultrasound sensor, the discrete Fourier transformation is used both on the

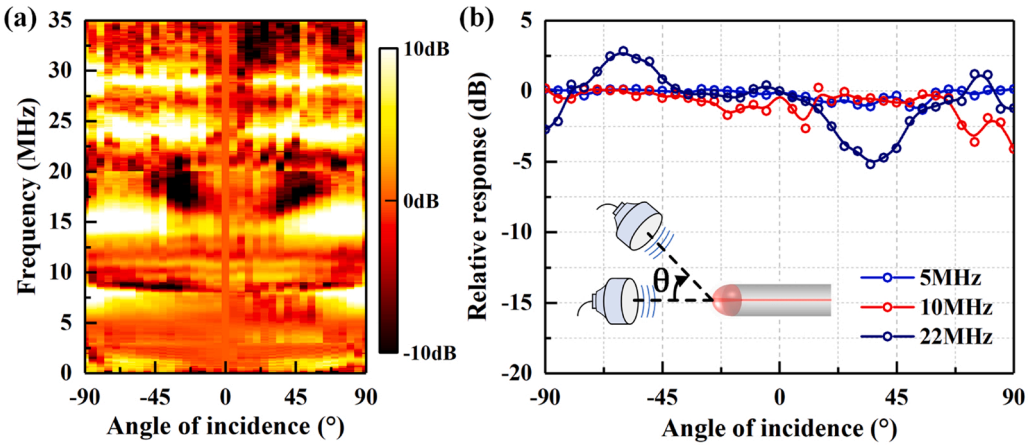

Fig. 4. (a) Measured directional response map of the fiber sensor. (b) Directional response at selected frequencies; inset: schematic of directional response measurement.

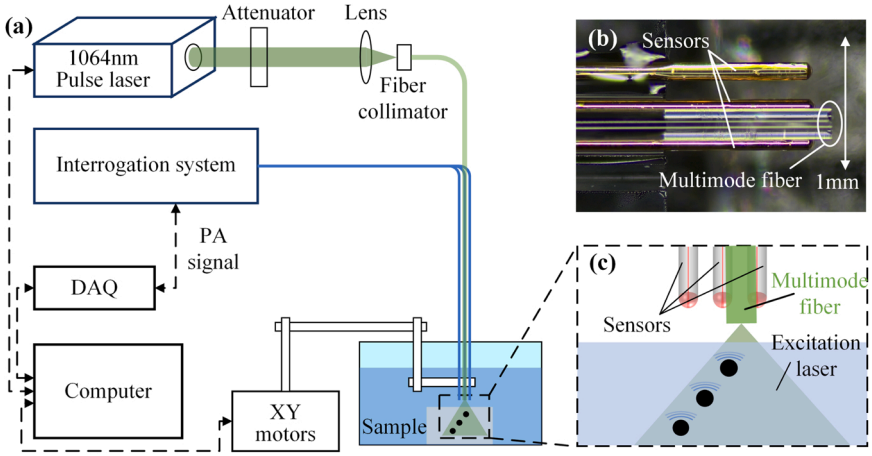

Fig. 5. (a) Schematic of the photoacoustic imaging system. Photograph (b) and schematic (c) of the photoacoustic imaging probe.

recorded temporal response waveforms measured by the fiber sensor and the calibrated PVDF needle hydrophone. The calibrated frequency response of needle hydrophone is used to correct the hydrophone measurements. Subsequently, the frequency curve measured by the fiber sensor is compared to the corrected curve thus obtaining the frequency response. The frequency response is measured using a planar broadband ultrasound source shown in Fig. 2(c), which is generated by illuminating a 6 ns pulsed laser on a black paint coating. The normalized frequency response of the fiber optic ultrasound sensor is shown in Fig. 3(c). The fiber sensor exhibits a wide bandwidth over 14 MHz with − 6 dB cut-off frequency. Notably, the fiber sensor exhibits an uneven frequency response due to sharp diffraction boundary of the fiber tip, which can be mitigated by using a rounded fiber tip.

Directivity response is of critical importance for imaging techniques such as photoacoustic tomography and diagnostic ultrasound imaging which employ back projection, phase array or other synthetic aperture methods. The directivity of the sensor is measured by using ultrasound transducers of 5 MHz, 15 MHz and 35 MHz within the frequency ranges of 0–8 MHz, 8–20 MHz and 35 MHz, respectively. As shown in the inset of Fig. 4(b), the transducers are rotated 180° around the fiber sensor with step of 5°. Fig. 4(a) depicts the measured directional response of the fiber sensor. The sensor exhibits a relatively flat response from − 90–90° when the frequency is less than 13 MHz. For comparison, the directional response of the hydrophone at the same frequency is less than ± 20°. Meanwhile, the fiber sensor also provides a superior directivity at higher frequencies. For example, the sensor's omnidirectional response fluctuation is less than ± 5 dB at 22 MHz, which is shown in the Fig. 4 (b).

4. Photoacoustic imaging

4.1. System setup

To demonstrate the applicability of the fiber optic ultrasound sensor for photoacoustic imaging, several samples are selected for imaging. To this end, a photoacoustic imaging system based on aperture synthesis is built. The imaging probe consists of two components as the multimode optical fiber for photoacoustic excitation and fiber optic ultrasound sensors for photoacoustic detection. As shown in Fig. 5(b), the ultrasound sensors are fixed in V groove with a spacing of 250 μm, and the imaging probe has an ultra-small size, which is less than 1 mm. The multimode optical fiber with a core diameter of 200 μm and a numerical aperture of 0.38 is used for a wide-angle photoacoustic excitation. A nanosecond Nd: YAG pulsed laser is employed as the excitation source. The excitation laser with a wavelength of 1064 nm and a pulse duration of 6 ns is coupled into the multimode fiber using a series of lens. The maximum fluence of the phantom surface is about 12 mJ/cm^2, which is below the American National Standards Institutes safety limit. To demodulate the output signal from the sensors, an interrogation system in Section 3.1 is developed. The measurement signals are digitalized and recorded by an oscilloscope with a sampling rate of 250 MHz. Two motors are assembled together to perform x- and y- direction scanning of

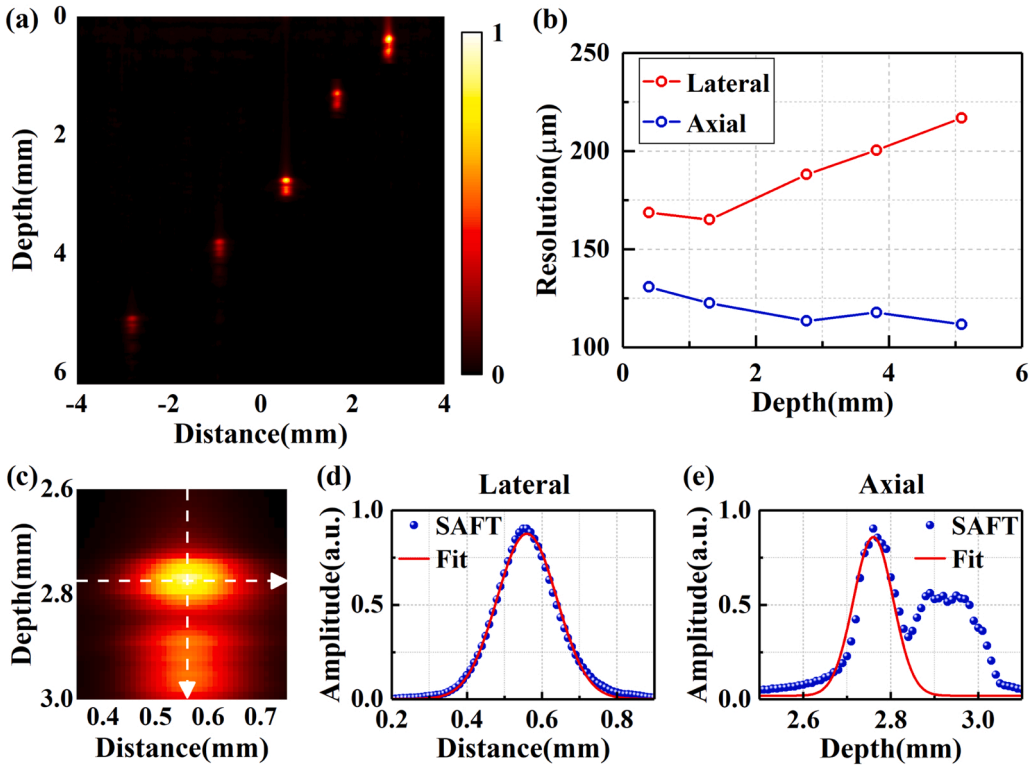

Fig. 6. (a) Photoacoustic image of human hairs at different depth. (b) Lateral and axial resolutions at different depths. (c) The expanded view of the reconstructed hairs at 2.8 mm depth. (d) Horizontal profile and Gaussian fitting curve of (c). (e) Vertical profile and Gaussian fitting curve of (c).

the imaging probe. A homemade LabVIEW program is used to control and synchronize excitation laser, motors and interrogation system. The excitation laser repetition frequency is 2 Hz. After data acquisition, the data is processed and reconstructed by MATLAB program.

4.2. Data processing and image reconstruction

Imaging reconstructed algorithm with excellent performance is the basis of high-resolution photoacoustic imaging. The high-resolution photoacoustic images are reconstructed by synthetic aperture focusing technique (SAFT) [32], which is commonly used in ultrasound imaging. Briefly, this is based on the standard delay-and-sum operation in the time domain for beam focusing to provide high lateral resolutions. The synthesized large aperture focusing signal is as follows:

$$S_{SAFT}(t) = \sum_{i=0}^{N-1} S(i, \quad t - \Delta t_i) \tag{3}$$

where $S(i,t)$ is the photoacoustic signal detected at the scanning position i, Δt_i denotes the time delay applied to the signal received at the scanning position i. N represents the total number of adjacent scanning lines included in SAFT summation. Generally, the coherence factor (CF), which is a real number ranging from 0 to 1, is used to further improve the focusing quality of SAFT images.

$$CF(t) = \frac{\left| \sum_{i=0}^{N-1} S(i, t - \Delta t_i) \right|^2}{N \sum_{i=0}^{N-1} |S(i, t - \Delta t_i)|^2} \tag{4}$$

By combining the SAFT data with the CF, the side lobes of SAFT image will be effectively suppressed.

4.3. Spatial resolution and imaging depth range

To characterize the lateral and axial resolutions of the photoacoustic imaging, five human hairs with diameter of 90 μm are used as the samples. The hairs were placed at five different depths at 0.5–5 mm. The imaging probe is interleaved scanned to achieve a spatial sampling interval of 10 μm. After signal acquisition, the CF-SAFT algorithm as described previously is applied to reconstruct the photoacoustic image, and Hilbert transform is further used along the z direction to acquire the signal envelope. Signals are not averaged during reconstruction. The reconstructed image is illustrated in Fig. 6(a) and the hairs are clearly visualized. The Fig. 6(c) is an expanded view of the third reconstructed hairs. A horizontal profile and a vertical profile are taken through the center of the reconstructed hair at representative depth of 2.8 mm. Gaussian functions are used to fit the profiles as shown in Fig. 6(d) and (e), respectively, and the resolutions can be determined by the full width at half maximum of the Gaussian curves. Consequently, the lateral and axial resolutions at different depths can be estimated as presented in Fig. 6(b). It can be seen that the lateral resolutions are 165–217 μm over the depth range of 5 mm. The lateral resolution is mainly determined by the size of synthetic aperture, which is determined by the overlap of the excitation laser illumination aperture and the acoustic detection aperture. With the increase of imaging depth, the synthetic aperture first increases and then decreases. Therefore, the lateral resolution first improves and then deteriorates with the increase of imaging depth. Meanwhile, the axial resolution of the imaging system is distributed in the range of 112–131 μm. The axial resolution variation depends on both of the size of synthetic aperture and the frequency response of the sensor. With the increase of imaging depth, the size of synthetic aperture firstly becomes dominate, and then, the frequency response of the sensor gradually becomes dominate, hence the axial resolution firstly increases and then tends to be constant.

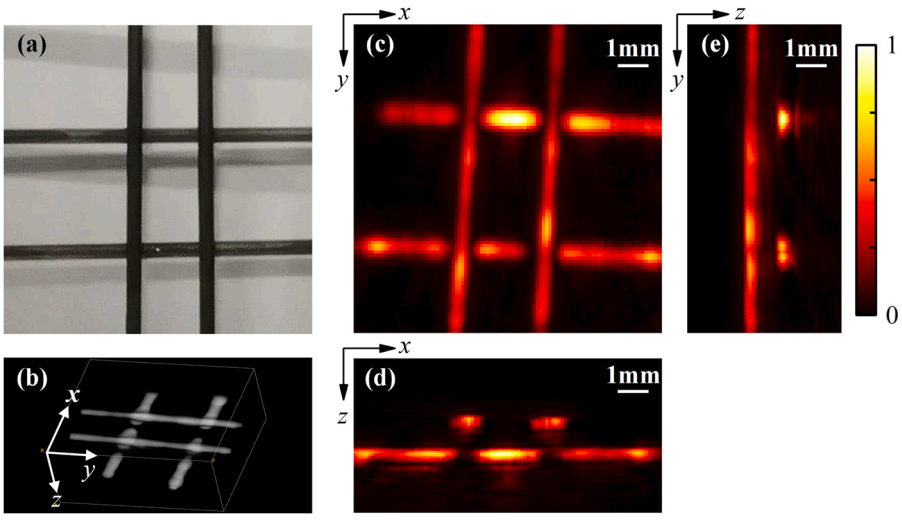

Fig. 7. Photograph (a) and 3D volume rendering PA image (b) of pencil leads phantom. Maximum intensity projection of the PA image in the x-y (c), x-z (d), and y-z (e) planes are provided.

4.4. Three-dimensional phantom imaging

A three-dimensional (3D) imaging experiment is carried out to further evaluate the performance of the photoacoustic imaging system. The phantom consists of four intersecting pencil leads at different depths, of which the photo is shown in Fig. 7(a). The imaging probe is raster scanned in a plane area of 10 mm × 10 mm with a space interval of 100 μm. A total number of $100 \times 100 = 10000$ PA signals are recorded for each tomogram. The two-dimensional (2D) CF-SAFT without signal average is employed for imaging reconstruction. Fig. 7 (b) shows the 3D volume rendering PA image and Fig. 7(c-e) show the maximum intensity projection (MIP) images of the reconstructed tomogram. It is clear that the four intersecting pencil leads are clearly visible and located at different depths. The results demonstrate the high-resolution 3D imaging capability of our photoacoustic imaging system. The total scanning time for an image is about 28 min, which is three times faster than using a single ultrasound sensor. The long data acquisition time is mainly limited by the following aspects. Firstly, the excitation laser has a low repetition rate of 2 Hz. Secondly, the imaging probe requires mechanical scanning, since only three ultrasound sensors are used. In the future, in vivo imaging can be realized by increasing the imaging speed, which is achieved by using an excitation laser with high repetition rate and parallel detection technology with hundreds of sensors.

5. Conclusion

In summary, we have reported a miniaturized fiber optic ultrasound sensor that is only 125 μm in diameter. Coherent demodulation system based on a fixed-wavelength laser combined with multiplexing technology is used to interrogate multiple sensors simultaneously. Meanwhile, the sensor also exhibits a broadband frequency response up to 14 MHz, a low NEP of 0.46 kPa and a near omnidirectional response. Furthermore, a photoacoustic imaging system is constructed based on the imaging probe, which consists of a multimode fiber and three fiber optic ultrasound sensors. With the help of CF-SAFT, high resolution 2D and 3D photoacoustic imaging over a lager depth range is achieved. The system exhibits high lateral resolutions of 165–217 μm and high axial resolutions of 112–131 μm, with a three-fold increase in imaging speed. The small size photoacoustic imaging probe is of great significance for high resolution endoscopic imaging of biological tissues.

Declaration of Competing Interest

The authors declare that they have no known competing financial interests or personal relationships that could have appeared to influence the work reported in this paper.

Data Availability

Data will be made available on request. The data that support the findings of this study are available from the corresponding authors upon reasonable request.

Acknowledgments

This work was supported by the National Natural Science Foundation for Distinguished Young Scholars (No. 61922033); Foundation for Innovative Research Groups of Hubei Province of China (2018CFA004); and Innovation Fund of WNLO.

References

[1] L.V. Wang, J. Yao, A practical guide to photoacoustic tomography in the life sciences, Nat. Methods 13 (2016) 627–638.
[2] A. Wiacek, M.A. Lediju Bell, Photoacoustic-guided surgery from head to toe [Invited], Biomed. Opt. Express 12 (2021) 2079–2117.
[3] P. Beard, Biomedical photoacoustic imaging, Interface Focus 1 (2011) 602–631.
[4] L.V. Wang, S. Hu, Photoacoustic tomography: in vivo imaging from organelles to organs, Science 335 (2012) 1458–1462.
[5] C. Lutzweiler, R. Meier, E. Rummeny, V. Ntziachristos, D. Razansky, Real-time optoacoustic tomography of indocyanine green perfusion and oxygenation parameters in human finger vasculature, Opt. Lett. 39 (2014) 4061–4064.
[6] J. Aguirre, M. Schwarz, N. Garzorz, M. Omar, A. Buehler, K. Eyerich, V. Ntziachristos, Precision assessment of label-free psoriasis biomarkers with ultra-broadband optoacoustic mesoscopy, Nat. Biomed. Eng. 1 (2017) 0068.
[7] P.K. Upputuri, M. Pramanik, Recent advances in photoacoustic contrast agents for in vivo imaging, Wiley Interdiscip. Rev. -Nanomed. Nanobiotechnol. 12 (2020), e1618.
[8] B.E. Treeby, E.Z. Zhang, B.T. Cox, Photoacoustic tomography in absorbing acoustic media using time reversal, Inverse Probl. 26 (2010), 115003.
[9] M. Pramanik, Improving tangential resolution with a modified delay-and-sum reconstruction algorithm in photoacoustic and thermoacoustic tomography, J. Opt. Soc. Am. A Opt. Image Sci. Vis. 31 (2014) 621–627.
[10] S. Ashkenazi, Y. Hou, T. Buma, M. O'Donnell, Optoacoustic imaging using thin polymer etalon, Appl. Phys. Lett. 86 (2005), 134102.
[11] J. Bauer-Marschallinger, K. Felbermayer, T. Berer, All-optical photoacoustic projection imaging, Biomed. Opt. Express 8 (2017) 3938–3951.
[12] J.A. Guggenheim, J. Li, T.J. Allen, R.J. Colchester, S. Noimark, O. Ogunlade, I. P. Parkin, I. Papakonstantinou, A.E. Desjardins, E.Z. Zhang, P.C. Beard, Ultrasensitive plano-concave optical microresonators for ultrasound sensing, Nat. Photon 11 (2017) 714–719.

[13] A. Hochreiner, J. Bauer-Marschallinger, P. Burgholzer, B. Jakoby, T. Berer, Non-contact photoacoustic imaging using a fiber based interferometer with optical amplification, Biomed. Opt. Express 4 (2013) 2322–2331.
[14] Y. Liang, L. Li, Q. Li, H. Liang, L. Jin, L. Wang, B.-O. Guan, Photoacoustic computed tomography by using a multi-angle scanning fiber-laser ultrasound sensor, Opt. Express 28 (2020) 8744–8752.
[15] B.-O. Guan, L. Jin, J. Ma, Y. Liang, X. Bai, Flexible fiber-laser ultrasound sensor for multiscale photoacoustic imaging, Opto-Electron. Adv. 4 (2021), 200081.
[16] B. Fischer, Optical microphone hears ultrasound, Nat. Photonics 10 (2016) 356–358.
[17] H. Chen, Z. Shao, Y. Hao, Q. Rong, A high-frequency hydrophone using an optical fiber microknot resonator, Opt. Commun. 446 (2019) 77–83.
[18] X. Bai, Y. Liang, H. Sun, L. Jin, J. Ma, B.O. Guan, L. Wang, Sensitivity characteristics of broadband fiber-laser-based ultrasound sensors for photoacoustic microscopy, Opt. Express 25 (2017) 17616–17626.
[19] L. Yang, C. Dai, A. Wang, G. Chen, D. Xu, Y. Li, Z. Yan, Q. Sun, Multi-channel parallel ultrasound detection based on a photothermal tunable fiber optic sensor array, Opt. Lett. 47 (2022) 3700–3703.
[20] G. Wissmeyer, D. Soliman, R. Shnaiderman, A. Rosenthal, V. Ntziachristos, All-optical optoacoustic microscope based on wideband pulse interferometry, Opt. Lett. 41 (2016) 1953–1956.
[21] P.C. Beard, T.N. Mills, Extrinsic optical-fiber ultrasound sensor using a thin polymer film as a low-finesse Fabry-Perot interferometer, Appl. Opt. 35 (1996) 663–675.
[22] W. Zhang, F. Chen, W. Ma, Q. Rong, X. Qiao, R. Wang, Ultrasonic imaging of seismic physical models using a fringe visibility enhanced fiber-optic Fabry-Perot interferometric sensor, Opt. Express 26 (2018) 11025–11033.
[23] A.P. Jathoul, J. Laufer, O. Ogunlade, B. Treeby, B. Cox, E. Zhang, P. Johnson, A. R. Pizzey, B. Philip, T. Marafioti, M.F. Lythgoe, R.B. Pedley, M.A. Pule, P. Beard, Deep in vivo photoacoustic imaging of mammalian tissues using a tyrosinase-based genetic reporter, Nat. Photon 9 (2015) 239–246.
[24] R. Ansari, E.Z. Zhang, A.E. Desjardins, P.C. Beard, Miniature all-optical flexible forward-viewing photoacoustic endoscopy probe for surgical guidance, Opt. Lett. 45 (2020) 6238–6241.
[25] R. Ansari, E.Z. Zhang, A.E. Desjardins, A.L. David, P.C. Beard, Use of a flexible optical fibre bundle to interrogate a Fabry-Perot sensor for photoacoustic imaging, Opt. Express 27 (2019) 37886–37899.
[26] R. Ansari, E.Z. Zhang, A.E. Desjardins, P.C. Beard, All-optical forward-viewing photoacoustic probe for high-resolution 3D endoscopy, Light Sci. Appl. 7 (2018) 75.
[27] H. Lamela, D. Gallego, A. Oraevsky, Optoacoustic imaging using fiber-optic interferometric sensors, Opt. Lett. 34 (2009) 3695–3697.
[28] X.D. Ma, Y.Q. Cai, B. Fu, L.J. Xu, J.G. Ma, Fiber optic-based laser interferometry array for three-dimensional ultrasound sensing, Opt. Lett. 44 (2019) 5852–5855.
[29] L. Yang, Y. Li, F. Fang, L. Li, Z. Yan, L. Zhang, Q. Sun, Highly sensitive and miniature microfiber-based ultrasound sensor for photoacoustic tomography, Opto-Electron. Adv. 5 (2022) 20076.
[30] J. Wang, F. Ai, Q. Sun, T. Liu, H. Li, Z. Yan, D. Liu, Diaphragm-based optical fiber sensor array for multipoint acoustic detection, Opt. Express 26 (2018) 25293–25304.
[31] E.Z. Zhang and P.C. Beard, Characteristics of optimized fibre-optic ultrasound receivers for minimally invasive photoacoustic detection, in *Conference on Photons Plus Ultrasound - Imaging and Sensing* , Proceedings of SPIE (Bellingham: SPIE, 2015), 932311.
[32] D. Cai, G. Li, D. Xia, Z. Li, Z. Guo, S.-L. Chen, Synthetic aperture focusing technique for photoacoustic endoscopy, Opt. Express 25 (2017) 20162–20171.

Liuyang Yang is currently a Ph.D. candidate in optical Engineering at the Huazhong University of Science and Technology. He received his B.S. from Huazhong University of Science and Technology. His research interests are fiber optic sensing and ultrasonic detection.

Dongchen Xu is currently a M.S. candidate in optical Engineering at the Huazhong University of Science and Technology. He received his B.S. from Huazhong University of Science and Technology. His research interests are in photoacoustic/ultrasonic dual-mode imaging system design and imaging algorithms.

Geng Chen obtained his B.S. in 2021 at Huazhong University of Science and Technology. He is currently a M.S. candidate in optical Engineering at the Huazhong University of Science and Technology. His research interest is the application of active fiber optic ultrasonic detection technology in nondestructive testing.

Anqi Wang is currently a Ph.D. candidate in optical Engineering at the Huazhong University of Science and Technology. She received her B.S. from Taiyuan University of Technology. Her research interest is in the medical application of fiber optic ultrasound detection technology.

Liangye Li obtained her B.S. in 2019 at Huazhong University of Science and Technology. She is currently a Ph.D. candidate in optical Engineering at the Huazhong University of Science and Technology. Her research interests are fiber optic sensing and human health monitoring.

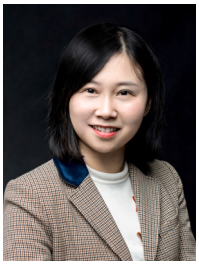

Qizhen Sun is a Professor of Optoelectronics at School of Optical and Electronic Information in Huazhong University of Science and Technology, and also the Director of Research Division of the Internet of Things Access in National Engineering Laboratory of Next Generation Internet Access System, China. She has a Ph.D. in Electronic Science and Technology from Huazhong University of Science and Technology. Her research spans optical fiber photonics, sensors and lasers and her work has been published in a number of different journal. She is an OSA senior member and IEEE member.